Article

Mobile-Phone Antenna Array with Diamond-Ring Slot Elements for 5G Massive MIMO Systems

Naser Ojaroudi Parchin [1],* [ID], Haleh Jahanbakhsh Basherlou [2] [ID],
Mohammad Alibakhshikenari [3] [ID], Yasser Ojaroudi Parchin [4], Yasir I. A. Al-Yasir [1] [ID],
Raed A. Abd-Alhameed [1] [ID] and Ernesto Limiti [3] [ID]

[1] Faculty of Engineering and Informatics, University of Bradford, Bradford BD7 1DP, UK;
    Y.I.A.Al-Yasir@bradford.ac.uk (Y.I.A.A.-Y.); R.A.A.Abd@bradford.ac.uk (R.A.A.-A.)
[2] Bradford College, Bradford BD7 1AY, UK; Hale.Jahanbakhsh@gmail.com
[3] Electronic Engineering Department, University of Rome Tor Vergata, Via del Politecnico 1, 00133 Rome, Italy;
    Alibakhshikenari@ing.uniroma2.it (M.A.); Limiti@ing.uniroma2.it (E.L.)
[4] Young Researchers and Elite Club, Germi Branch, Islamic Azad University, Germi 63764-56517, Iran;
    y.ojaroudi@gmail.com
* Correspondence: N.OjaroudiParchin@Bradford.ac.uk; Tel.: +44-7341436156

check for
updates

Abstract: A design of mobile-phone antenna array with diamond-ring slot elements is proposed for fifth generation (5G) massive multiple-input/multiple-output (MIMO) systems. The configuration of the design consists of four double-fed diamond-ring slot antenna elements placed at different corners of the mobile-phone printed circuit board (PCB). A low-cost FR-4 dielectric with an overall dimension of 75×150 mm^2 is used as the design substrate. The antenna elements are fed by 50-Ohm L-shaped microstrip-lines. Due to the orthogonal placement of microstrip feed lines, the diamond-ring slot elements can exhibit the polarization and radiation pattern diversity characteristic. A good impedance bandwidth ($S_{11} \leq -10$ dB) of 3.2–4 GHz has been achieved for each antenna radiator. However, for $S_{11} \leq -6$ dB, this value is 3–4.2 GHz. The proposed design provides the required radiation coverage of 5G smartphones. The performance of the proposed MIMO antenna design is examined using both simulation and experiment. High isolation, high efficiency and sufficient gain-level characteristics have been obtained for the proposed MIMO smartphone antenna. In addition, the calculated total active reflection coefficient (TARC) and envelope correlation coefficient (ECC) of the antenna elements are very low over the whole band of interest which verify the capability of the proposed multi-antenna systems for massive MIMO and diversity applications. Furthermore, the properties of the design in Data-mode/Talk-mode are investigated and presented.

Keywords: 5G; diamond-ring slot; dual-polarized antenna; massive MIMO; mobile-phone antenna; pattern diversity

1. Introduction

Nowadays, there is an increased interest in research on MIMO systems in wireless communication [1,2]. It has incomparable advantages in improving the wireless link transmission capacity and reliability. In MIMO systems, multiple antennas are deployed at both transmitter and receiver sides [3]. This technology is a key component and probably the most established to truly reach the promised transfer data rates of fifth generation (5G) communication systems [4,5]. MIMO antennas are important for increasing channel capacity and link reliability [6,7]. Standard MIMO networks tend to use two or four antennas in a single physical package. However, massive MIMO is a MIMO system with an especially high number of antennas [8]. A 2×2 MIMO system has been successfully applied

for fourth generation (4G) mobile communications and it is expected that the massive MIMO system with a large number of MIMO antennas is very promising for 5G wireless communications [9]. The greater number of elements in a network will make it more resistant to interference and intentional jamming [10].

Among the antennas which are used for MIMO applications, printed antennas are more appropriate due to their low cost, easy fabrication and their capability of easily being integrated to small terminal devices [11]. However, placing multiple antennas in the limited space of a transceiver poses a significant challenge in the incorporation of the MIMO technique. According to the requirement of cellular communications, compact, wideband and high isolation MIMO antenna is an urgent demand in the future mobile terminal and the portable applications [12–17]. Recently, several techniques have been introduced to design massive MIMO antennas for 4G and sub-6 GHz 5G mobile terminals [18–27].

We propose here a new design of Eight-port mobile-phone antenna with compact dual-polarized radiation elements providing wide impedance bandwidths for 5G applications. Eight-element MIMO smartphone antenna can achieve the channel capacity of 37 bps/Hz which is close to eight times that of a single antenna for single-input/single-output operation. With such a channel capacity and a wide frequency spectrum (200 MHz, at least), the data rate can be much higher than 1 Gbps. The antenna is designed to operate at 3.6 GHz, a candidate frequency band for sub-6-GHz 5G cellular networks, proposed by Ofcom, UK [28]. The design configuration contains four elements of double-fed/dual-polarized slot-ring antennas placed at corners of the printed circuit board (PCB). The antenna elements exhibit wide impedance bandwidth with low mutual coupling function providing pattern and polarization diversity characteristics at different sides of the mobile-phone PCB. As a result, the design not only can provide full radiation coverage but also it can support different polarizations. The computer simulation technology (CST) software was used to investigate antenna characteristics [29]. Fundamental properties of the single-element and its MIMO design in terms of S parameters, efficiency, radiation pattern, envelope correlation coefficient (ECC), total active reflection coefficient (TARC) are investigated. In addition, the performance of the designed mobile-phone antenna in Data-Mode/Talk-Mode are studied.

2. Single-Element Diamond-Ring Slot Antenna

Figure 1 depicts the configuration of the dual-polarized diamond-ring antenna. The antenna is designed on an FR-4 substrate (h = 1.6 mm, ε = 4.4, and δ = 0.025).

Its configuration contains a diamond-ring slot radiator with a pair of L-shaped microstrip feed lines. Parameter values of the designed antenna and its MIMO configuration are specified in Table 1. The motive behind the presented design is to achieve a dual-polarized wideband antenna with compact-size and capability of integration onto smartphone PCB. This has been achieved by using the diamond-ring slot antenna with L-shaped microstrip feed lines. The slot antenna is one type of printed antenna that has been investigated extensively for different wireless systems for several decades because of its attractive features including light-weight, compactness and ease of integration with radio frequency (RF) circuit [30]. The ring-slot antenna can excite two orthogonal polarization if it is fed differently [31]. This makes the printed-ring-slot antennas attractive. The resonant frequency of the antenna is mainly determined by the circumference length of the employed diamond-ring slot. Therefore, the circumference length of the diamond-ring slot needs to satisfy the dielectric wavelength at the corresponding frequency point, where $W_x/2 + g = \lambda$. However, the length of feed-line ($L_f + L_1$) also has a little effect on the frequency point and impedance-bandwidth of the design.
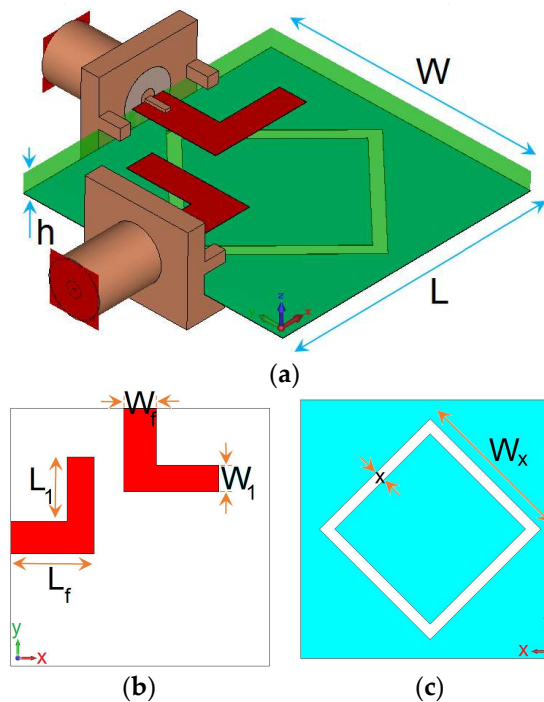
Figure 1. The antenna schematic, (**a**) side view, (**b**) top and (**c**) bottom layers.

Table 1. Parameter values of the single-element antenna and its MIMO array design.

Parameter	Value (mm)	Parameter	Value (mm)	Parameter	Value (mm)	Parameter	Value (mm)
W_S	75	L_S	150	x	1	W	24
L	24	W_f	3	L_f	5.25	W_1	2.5
L_1	3.9	W_2	8.9	L_2	9.9	W_x	7.25

Configurations and S parameters of the square-ring slot with rectangular feed line, a diamond-ring slot with rectangular feed line, and the proposed diamond-ring slot radiator with L-shaped feed line are illustrated and compared in Figure 2a–c, respectively. It can be observed that by using the proposed design (Figure 2c), the antenna not only provides wider impedance bandwidth but it also exhibits high isolation with low mutual coupling characteristic (less than −20 dB) at the desired operation band. As shown, the operation frequency of the slot radiator with L-shaped feed lines spans from 3.2 to 4 GHz (800 MHz bandwidth). For $S_{11} \leq -6$ dB, this value is 3–4.2 GHz.

S_{11} characteristics of varying design parameters including W_x, L_1, x and W_1 are illustrated in Figure 3. Figure 3a depicts the effects of diamond-ring size (W_x) on the resonance frequency: when its size decreases from 8 to 6 mm, the antenna resonance varies from 3.2 to 4.6 GHz. The frequency resonance of the antenna is also affected by the size of the L-shaped feed line arm (L_1). As shown in Figure 3b, the antenna operation frequency tunes to lower frequencies (without any changes on its bandwidth or isolation). Figure 3c illustrates the S_{11} results for various values of x (width of the diamond-ring slot-line). As shown, it mainly affects the impedance bandwidth of the antenna: when its size changes from 0.5 to 2 mm, the antenna operation bandwidth varies from 0.3 to 1.2 GHz. Another important parameter of the dual-polarized diamond-ring slot antenna design is the length of the feed line arm (L_1) which tunes the isolation characteristic. As can be observed from the results shown in Figure 3d, the antenna reflection coefficient tunes from −18 to less than −40 dB.
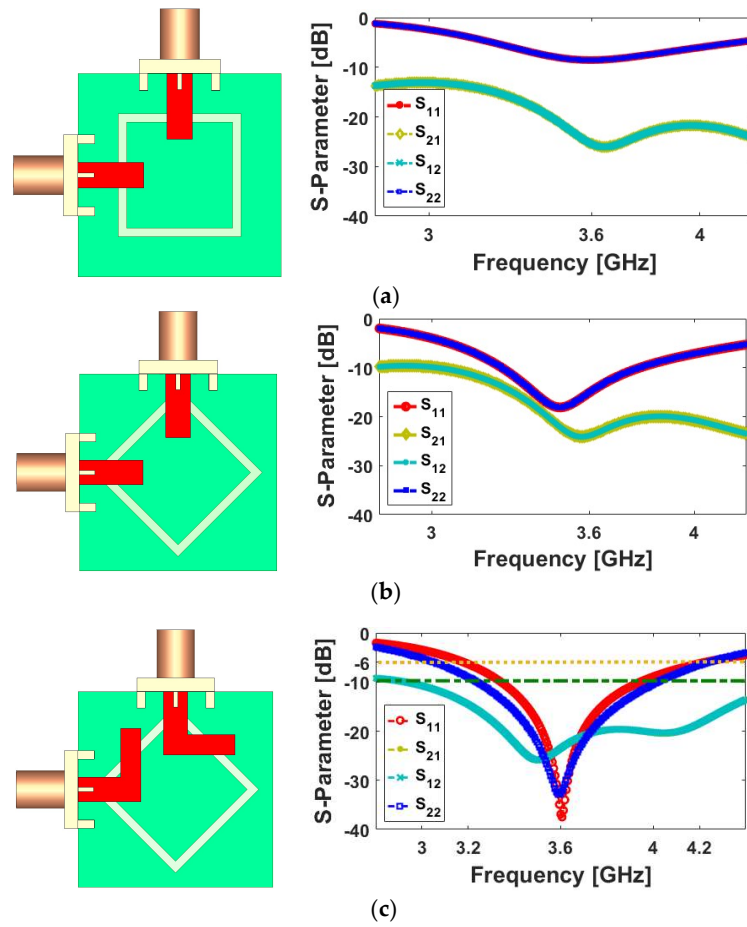
Figure 2. Various structures and S parameter results of: (**a**) square-ring slot with rectangular feed line, (**b**) diamond-ring slot with rectangular feed line, and (**c**) the proposed diamond-ring slot radiator with L-shaped feed line.
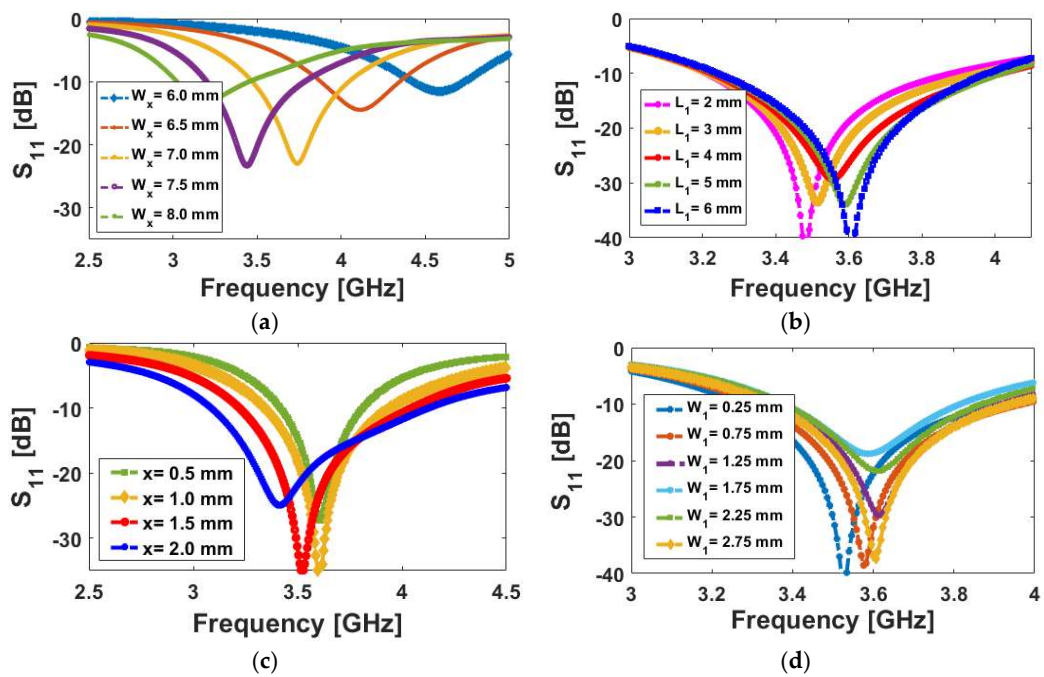

Figure 3. S_{11} results of the diamond-ring antenna for various values of (**a**) W_x, (**b**) L_1, (**c**) x, and (**d**) W_1.

Figure 4 shows the surface current distributions in the ground plane of the antenna at 3.6 GHz. As shown, the surface currents are mainly distributed around the diamond-ring slot radiator. In addition, for the different feeding ports of the antenna, the currents densities are equal and opposite due to the polarization diversity function [32–34]. Figure 5 illustrates the 3D radiation patterns of the antenna when it is fed differently (Port 1 and Port 2). As seen, the antenna exhibits similar radiation patterns with different orthogonal polarizations and more than 3 dB realized-gain. Radiation characteristics of the dual-polarized diamond-ring slot antenna in terms of radiation efficiency, total efficiency, and maximum gain are illustrated in Figure 6. As seen, the antenna provides high efficiencies. More than 80% radiation and total efficiency properties are obtained over the entire operation band (3.2–4 GHz). It can be observed that the antenna exhibits almost similar radiation and total efficiency. In addition, the antenna has around 2.5 dBi directivity.
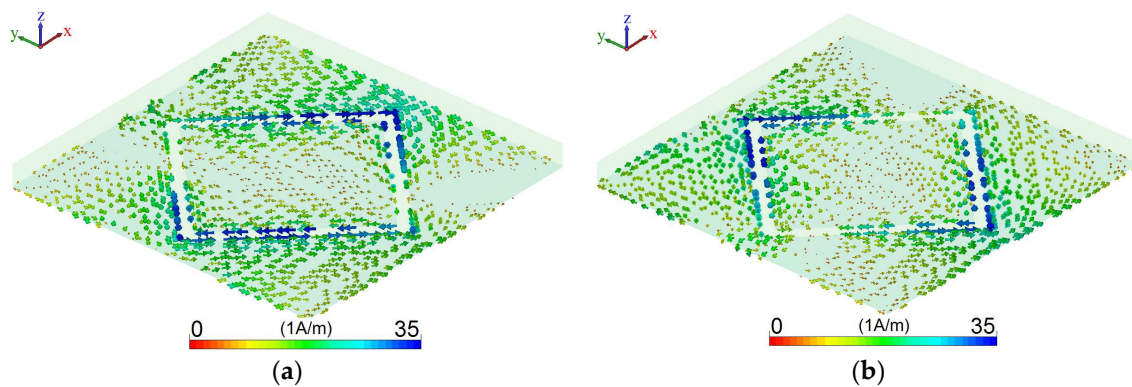

Figure 4. Simulated current densities at 3.6 GHz for (**a**) 1st feeding port and (**b**) 2nd feeding port.
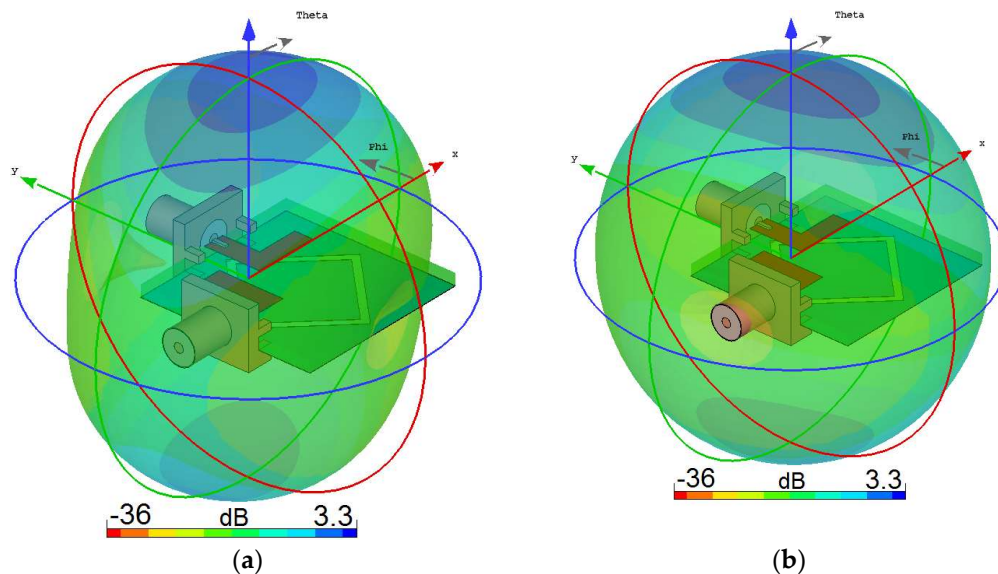

Figure 5. 3D views of the dual-polarized radiation patterns from (**a**) feeding port 1 and (**b**) feeding port 2.

A prototype of the design was fabricated and its S parameters were tested. Figure 7 shows a photograph of the fabricated prototype in the measurement setup. Figure 8 illustrates the measured and simulated S parameter results of the fabricated antenna. It is observed that the fabricated antenna works properly at the desired frequency range.
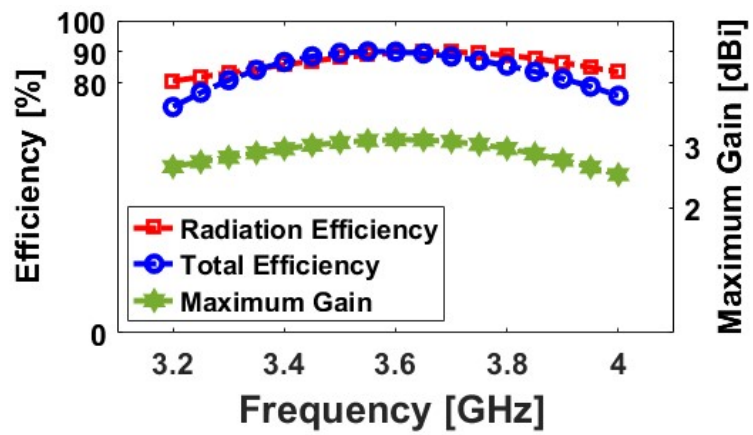
Figure 6. Radiation, total efficiencies, maximum gain of the diamond-ring slot antenna.
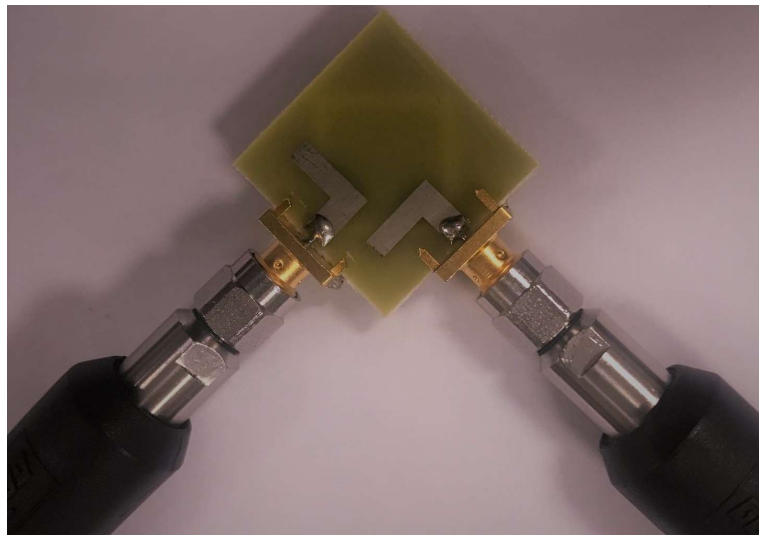

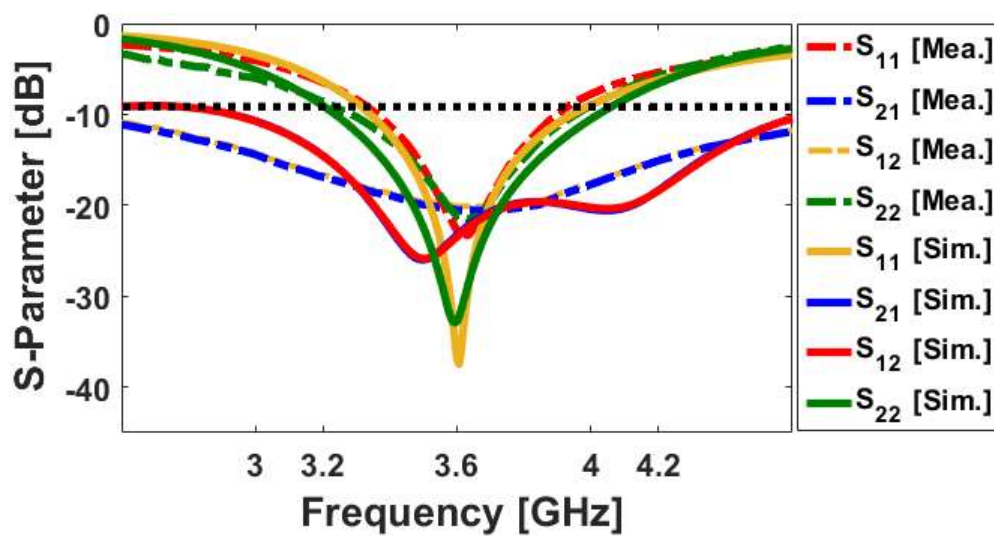**Figure 7.** Photograph of the fabricated prototype in the measurement setup.

Figure 8. Measured and simulated S parameter results of the fabricated antenna.

3. Mobile-Phone Antenna Design

The simulated design layout of the mobile-phone antenna design is shown in Figure 9. It was implemented on an FR4 substrate with an overall dimension of 75×150 mm^2. Four elements of the dual-polarized diamond-ring slot radiators are employed at the corner of the mobile-phone PCB. As can be observed, due to the compact size of the employed radiator, there is enough spaces in the configuration of smartphone antenna PCB to add other antennas covering different frequencies of 3G/4G mobile terminals. Figure 10 illustrates the simulated S parameters (including S_{nn} and S_{mn}) of the design over its operation band. It is evident that the proposed mobile-phone antenna exhibits good S parameters with wide bandwidth and low mutual coupling characteristics. As mentioned above, the dual-polarized radiation elements provide similar performances. 3D radiation patterns of antennas 1 and 2 at 3.6 GHz is represented in Figure 11. As seen, the antenna elements have quasi-omnidirectional radiation patterns covering the top and bottom portions of the mobile-phone PCB.
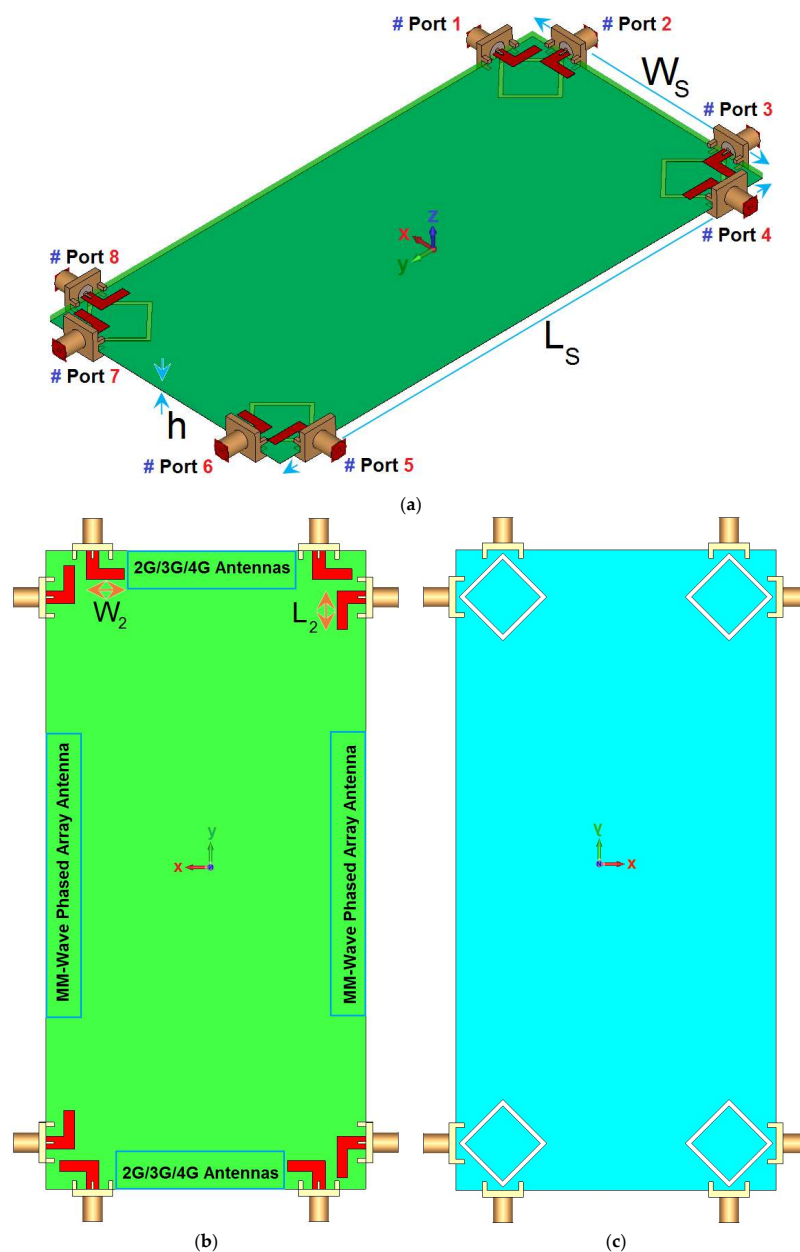

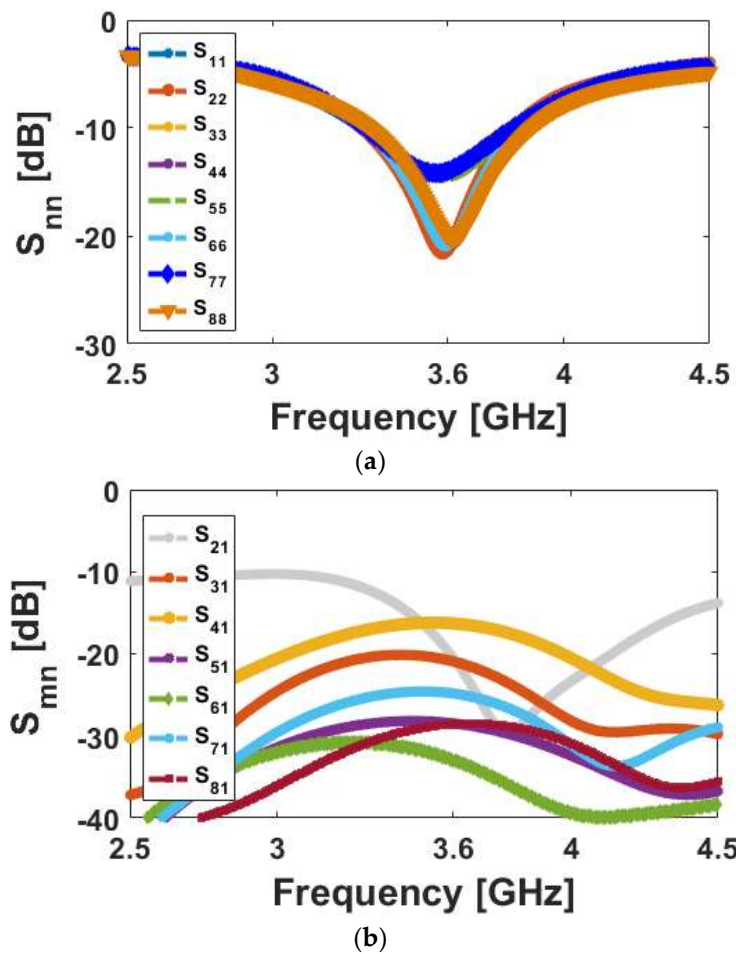**Figure 9.** Designed mobile-phone antenna (**a**) transparent view, (**b**) top-layer and (**c**) bottom layer.

(a)

(b)

Figure 10. (**a**) S_{nn} and (**b**) S_{mn} results of the mobile-phone antenna.
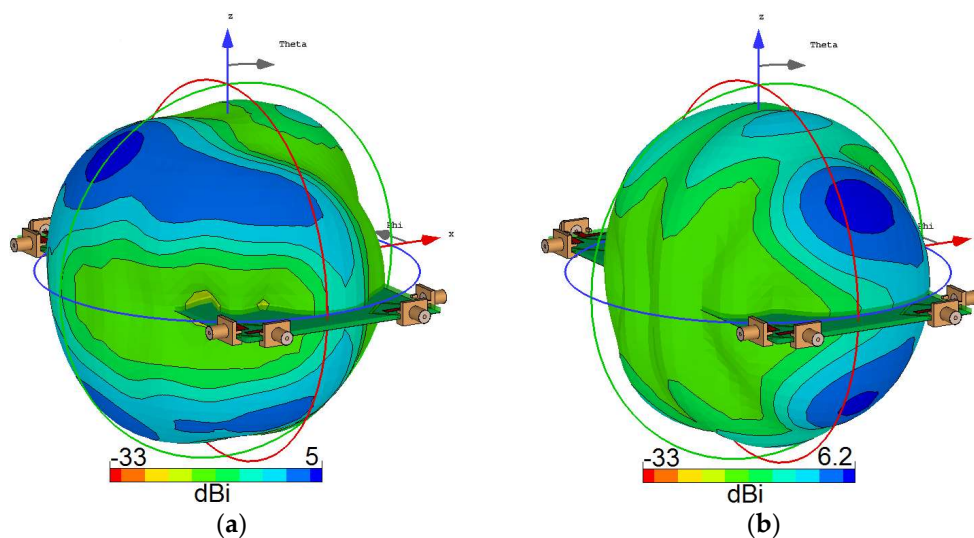

(a)　　　　　　　　　　　　　　　　(b)

Figure 11. 3D transparent views of the radiation patterns for (**a**) feeding port 1 and (**b**) feeding port 2.

Top-views of the radiation patterns for the proposed mobile-phone antenna design are displayed in Figure 12. It can be seen that each side of the mobile-phone PCB has been covered with differently polarized radiation patterns. Thus, the MIMO antenna exhibited good radiation coverage and can support different polarizations which make it more suitable to be used in future smartphones. Furthermore, the antenna provides high radiation and total efficiencies over the operation band, as

illustrated in Figure 13: more than 70% radiation and total efficiencies were obtained for the radiation elements at 3.6 GHz.

The proposed mobile-phone antenna was fabricated and its characteristics were tested in the Antenna Laboratory at the University of Bradford. Top and bottom views of the prototype are shown in Figure 14a,b, respectively. The mobile-phone antenna is constructed on a cheap FR4 dielectric with an overall dimension of $75 \times 150 \times 1.6$ mm^3. During the measurement process, 50-Ω RF loads are employed for the elements not under test to avoid their effects, as shown in Figure 14c. The measured and simulated S parameters (S_{nn}: S_{11}–S_{88} and S_{mn}: S_{21}–S_{81}) of the fabricated design are illustrated in Figure 15. As illustrated, the diamond-ring slot resonators achieve good S parameters with sufficient impedance bandwidth and low mutual coupling characteristic in the desired frequency range. Some deviations from the measurements arise from the errors in fabrication, feeding and experiment processes.
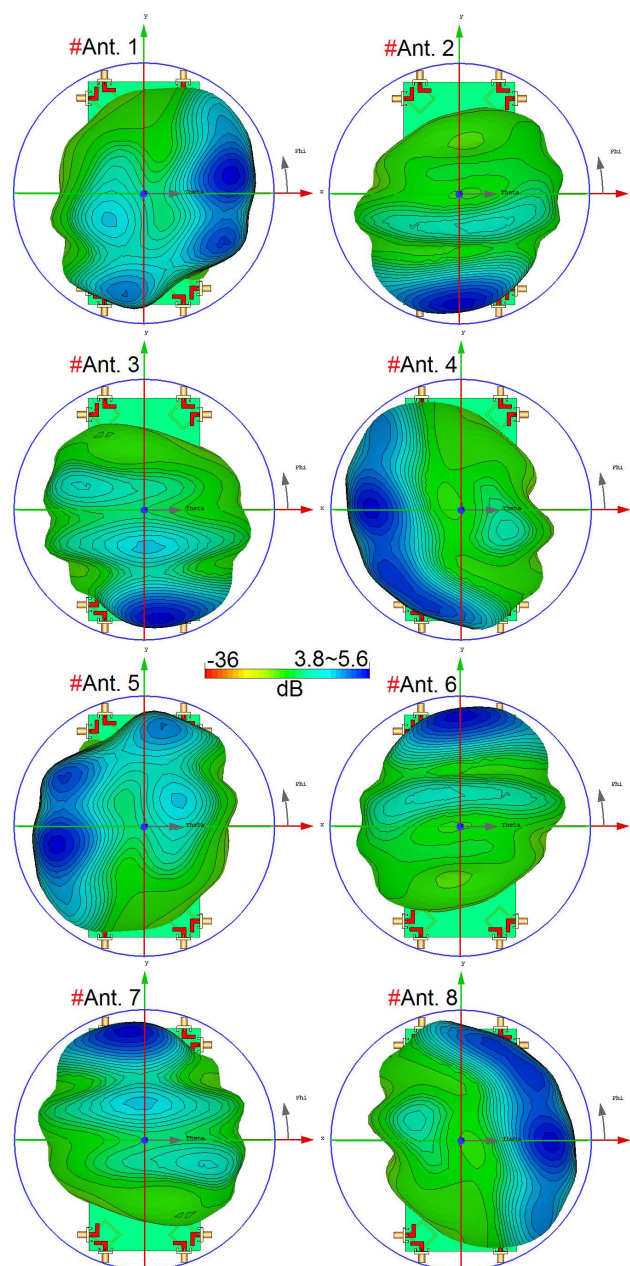

Figure 12. 3D radiation patterns of the fifth generation (5G) mobile-phone antenna.

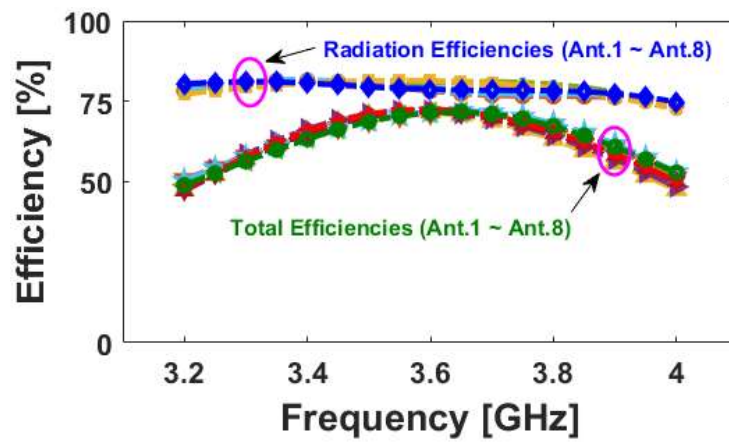**Figure 13.** Efficiencies of the antenna elements (Ant. 1–Ant. 8) for the proposed design.
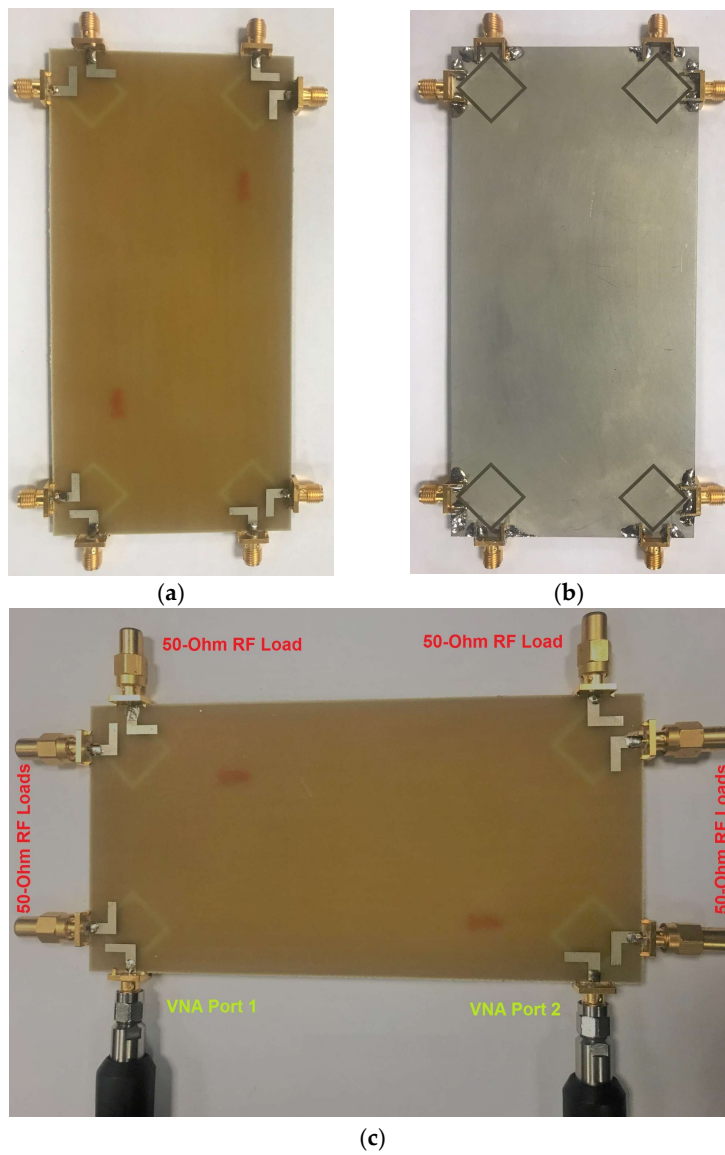

(**a**)

(**b**)

(**c**)

Figure 14. (**a**) Top, (**b**) bottom views of the fabricated design and (**c**) the prototype connected to the cables and 50-Ohm loads.
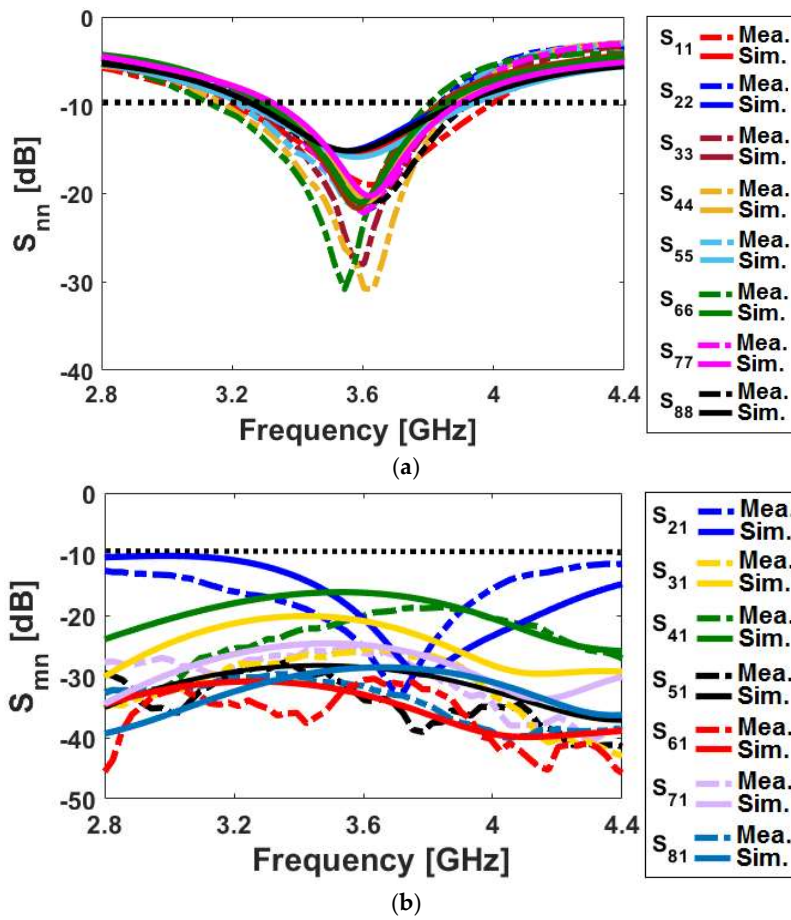
Figure 15. Measured and simulated (**a**) S_{nn} (S_{11}–S_{88}) and (**b**) S_{mn} (S_{21}–S_{81}) of the fabricated prototype.

According to the point that the radiation elements with the same placements and polarizations provide similar radiation patterns, 2D polar radiation patterns of the adjacent resonators (including Ant. 1 and Ant. 2) were measured at center operating frequency (3.6 GHz) and illustrated in Figure 16. As shown, the sample prototype exhibits good radiation patterns and provides acceptable agreement with simulations. In addition, the antenna elements with different polarizations provide sufficient gain values at the center frequency of the operation band.
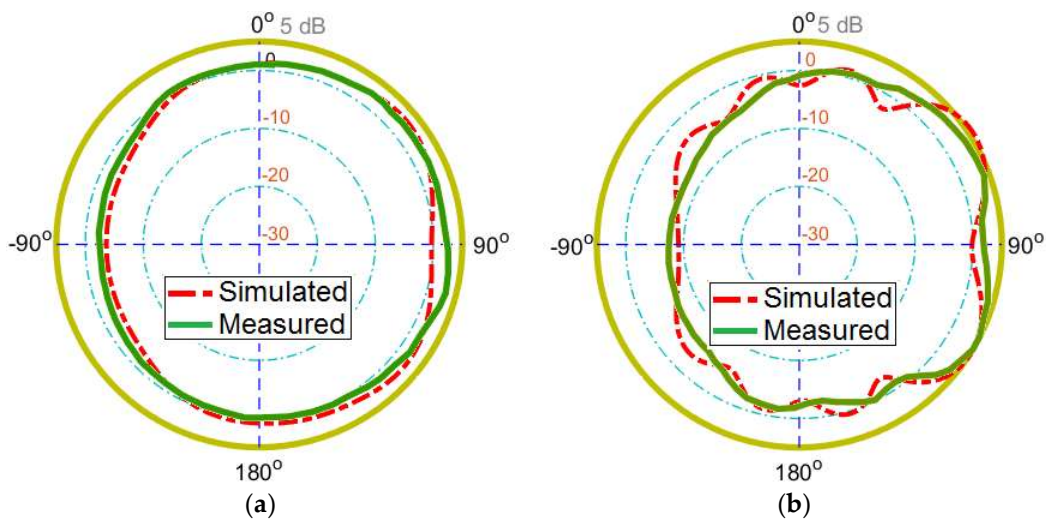

Figure 16. Measured and simulated 2D radiation patterns for (**a**) Ant.1 and (**b**) Ant.2.

In order to ensure that the MIMO antenna can work properly, ECC and TARC characteristics are two important parameters which should be considered in MIMO antennas [35,36]. The ECC and TARC of two elements can be calculated from the S parameters using the formula described as:

$$ECC = \frac{\left|S_{mm}^{*}S_{nm} + S_{mn}^{*}S_{nn}\right|^{2}}{\left(1 - |S_{mm}|^{2} - |S_{mn}|^{2}\right)\left(1 - |S_{nm}|^{2} - |S_{nn}|^{2}\right)^{*}}, \tag{1}$$

$$TARC = -\sqrt{\frac{(S_{mm} + S_{mn})^{2} + (S_{nm} + S_{nn})^{2}}{2}}. \tag{2}$$

Figure 17 shows the calculated ECC and TARC results from simulated and measured S parameters of the mobile-phone antenna design. As evident from figures, the calculated ECC and TARC results are very low over the whole band of interest. The design provides less than 0.01 ECC over the entire operating band and proves that two adjacent antenna elements are irrelevant. In addition, its TARC value is less than −30 at 3.6 GHz. Table 2 summarizes and compares the fundamental characteristics of the presented mobile-phone antenna with the recently reported 5G mobile-phone antenna designs [16–25]. It can be observed that the proposed design can provide better performances in terms of efficiency, isolation and ECC. In addition, it exhibits wider bandwidth with pattern and polarization diversity characteristics to cover different sides of the mobile-phone PCB.
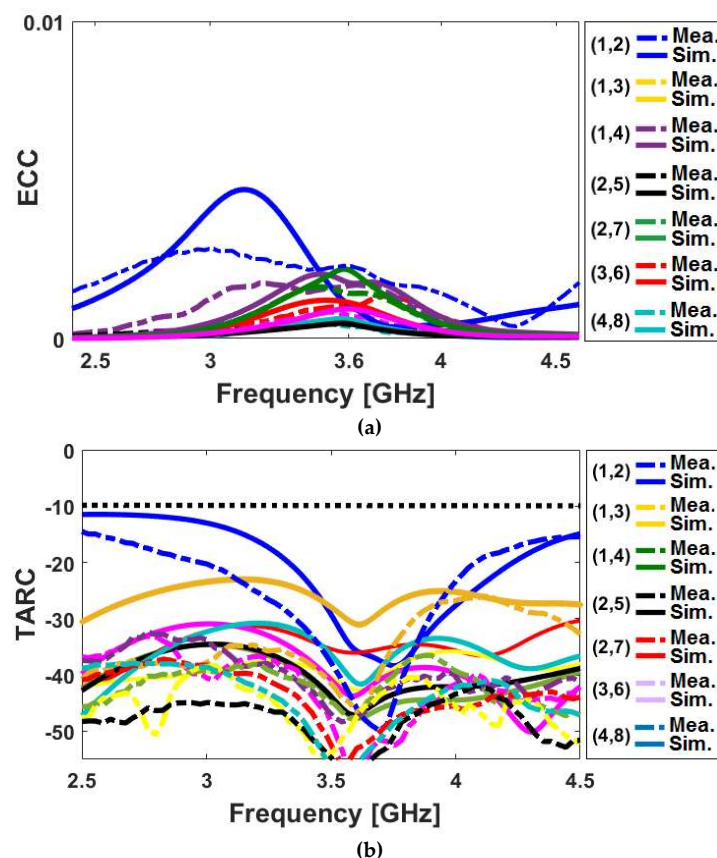

Figure 17. Calculated (**a**) envelope correlation coefficient (ECC) and (**b**) total active reflection coefficient (TARC) from measured S parameters.

Table 2. Comparison between the presented and recently reported 5G mobile-phone antennas.

Reference	Bandwidth (GHz)	Efficiency (%)	Size (mm^2)	Isolation (dB)	ECC
[18]	3.4–3.6	55–60	100×50	10	-
[19]	3.4–3.6	-	136×68	15	-
[20]	3.55–3.65	52–76	150×75	11	-
[21]	3.4–3.6	35–50	150×75	11	<0.40
[22]	3.4–3.6	30–50	145×70	15	<0.2
[23]	3.4–3.6	40–60	136×68	14	<0.2
[24]	3.4–3.6	60–75	150×80	17	<0.05
[25]	3.4–3.6	50–70	150×73	17	<0.07
[26]	3.4–3.6	50–80	150×75	15	<0.2
[27]	3.4–3.6	60–70	150×75	18	<0.015
Proposed	3.3–3.9	60–80	150×75	17	<0.01

4. User-Hand/User-Head Impacts on the Mobile-Phone Antenna Performance

The impact of human-hand/human-head on the characteristics of the design in terms of total efficiency and antenna realized-gain were investigated in this section [37–39]. As illustrated in Figure 18, different scenarios including right-hand and left-hand modes for top-layer and back-layer of the design are studied in simulations. According to the obtained results, the mobile-phone antenna design and its radiators exhibit good performances and provide sufficient total efficiencies in the presence of the human hand. Due to the symmetric configuration of the proposed design, it performs almost similarly for different hand scenarios. The maximum reductions of the radiation properties are observed for the radiation elements partially covered by the user hand which is due to the nature of hand tissue properties which can highly absorb the radiation power. As can be observed, the antenna elements provide 25–55% total efficiencies over the operation band of 3.2–4 GHz.
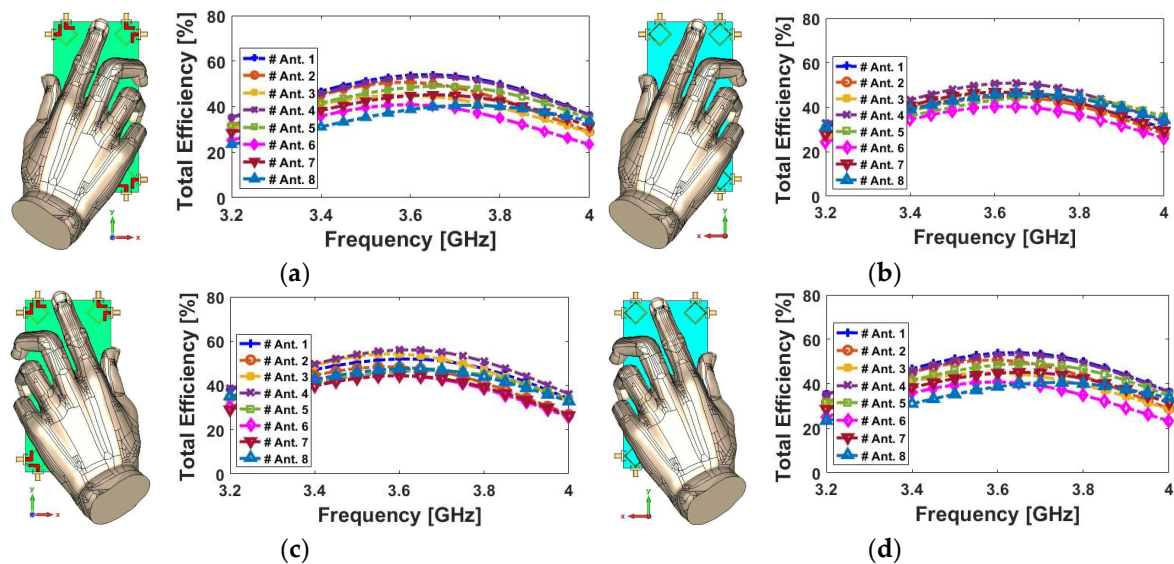

Figure 18. Placement and total efficiencies of the design for different user-hand scenarios (**a**) right-hand/top-layer, (**b**) right-hand/back-layer, (**c**) left-hand/top-layer and (**d**) left-hand/back-layer.

3D radiation patterns of the mobile-phone antenna in Talk-Mode at 3.6 GHz are illustrated in Figure 19a. It should be noted that the radiation performance of each antenna element mainly depends on its locations in the Talk-Mode scenario. As shown, the realized gain characteristic of the design varies from 3.2 to 4.9 dB. Compared with the radiation patterns in free space (Figure 12), due to the existence of the user's head and hand, radiation patterns are a bit distorted and become weaker. One

can see that antenna elements are touched by different parts of the hand and head phantoms in the presented Talk-Mode.
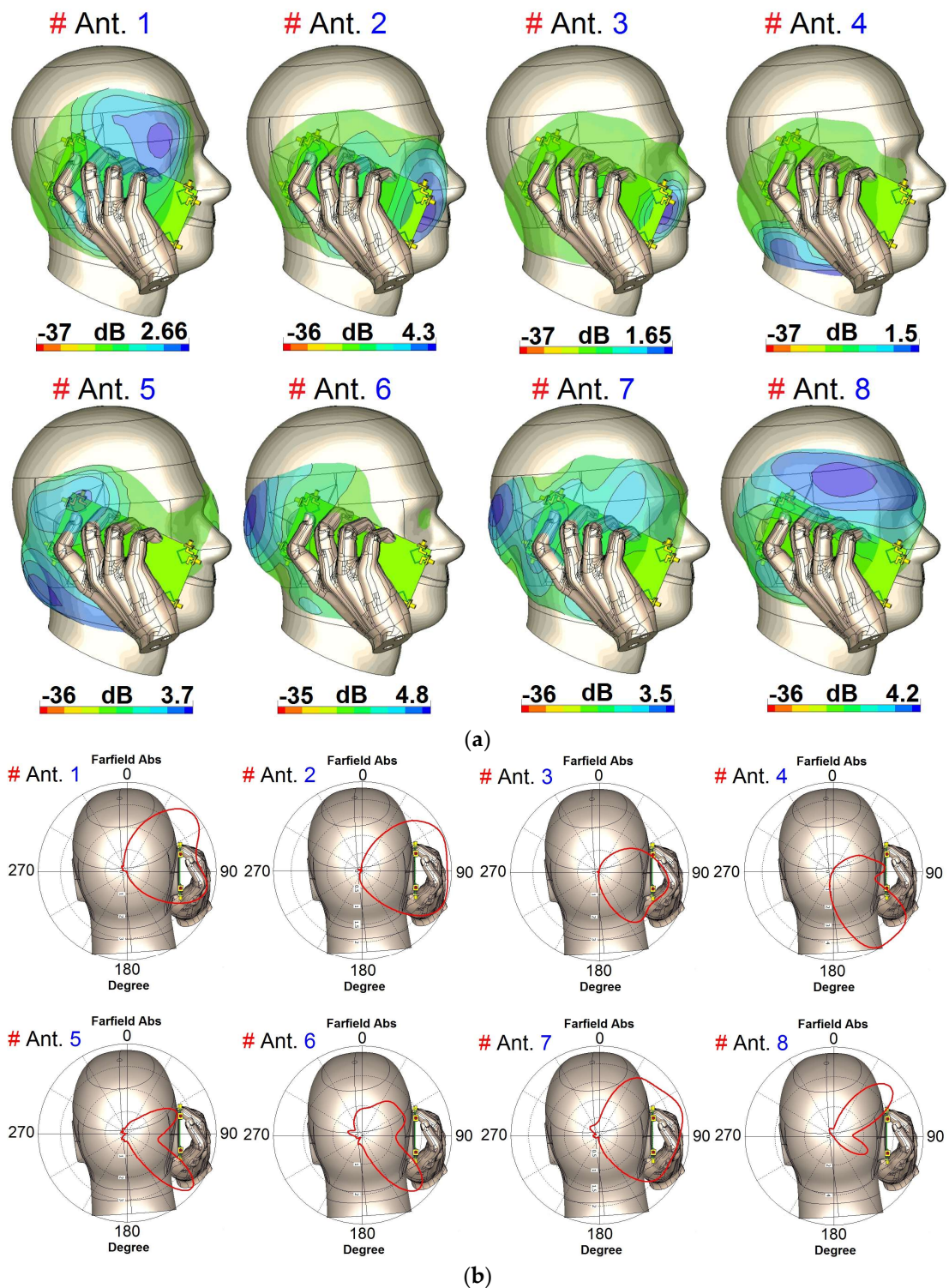

(**a**)

(**b**)

Figure 19. (**a**) 3D and (**b**) 2D linearly-scaled radiation patterns of the mobile-phone antenna in Talk-Mode scenario.

The maximum reductions of the radiation properties are observed for the elements that are located near to user-head (Ant. 3 and Ant. 4) [40]. However, the difference is not very significant. The 2D-polar

(linear-scaling) radiation patterns of the design are illustrated in Figure 19b. As can be observed, the directivity of the antenna radiation pattern is maximum in the opposite direction of the head, which is most important part of the body to protect from the radiation. The main lobe of each single-element directs most of the power while the other lobes should be negligible.

Figure 20 depicts the total efficiencies and reflection coefficient (S_{nn}) of the antenna elements in the presence of the user-head and user-hand in Talk-Mode scenario. As seen, the diversion of the S_{nn} characteristic of the design is not significant. In addition, the proposed MIMO design exhibit sufficient efficiency in its operation bandwidth. Based on the above analysis, we can conclude the MIMO design provides sufficient efficiency, radiation coverage and gain levels for diamond-ring slot radiators.
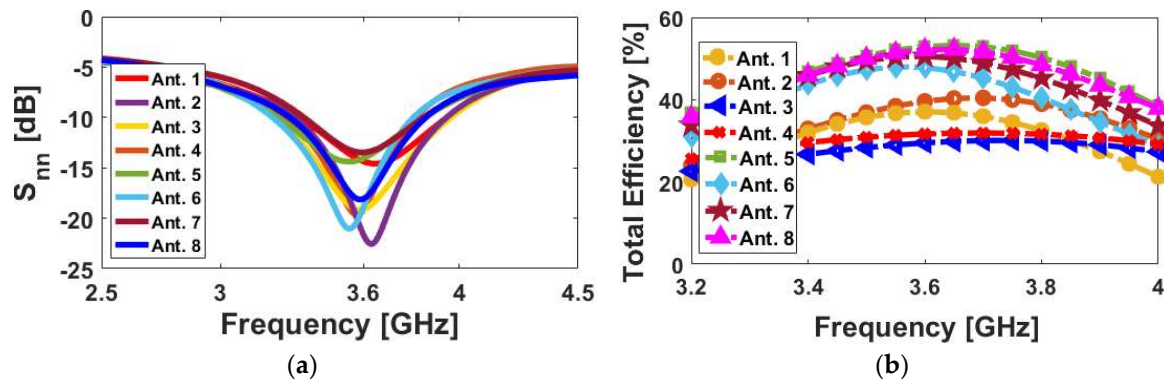

Figure 20. (**a**) S_{nn} and (**b**) total efficiencies of the proposed smartphone antenna in Talk-Mode scenario.

5. Conclusions

A mobile-phone antenna design with dual-polarized radiators is proposed for 5G massive MIMO communications. The antenna configuration contains eight-port/four elements of diamond-rings slot radiators with L-shaped microstrip feed lines deployed at four corners of the PCB. The antenna elements exhibit wide bandwidth with the center frequency of 3.6 GHz. S parameters, radiation patterns, efficiency, ECC and TARC results of the design are studied and sufficient results are achieved. In addition, a prototype of the mobile-phone antenna was fabricated and measured. Moreover, the performances of the antenna in Hand-Mode and Talk-Mode scenarios are investigated. The obtained results demonstrated that the proposed smartphone antenna provides good characteristics and meets the requirements for use in future mobile handsets.

References

1. Jensen, M.; Wallace, J. A review of antennas and propagation for MIMO wireless communications. *IEEE Trans. Antennas Propag.* **2004**, *52*, 2810–2824. [CrossRef]
2. Gesbert, D.; Shafi, M.; Shiu, D.S.; Smith, P.J.; Naguib, A. From theory to practice: An overview of MIMO space-time coded wireless systems. *IEEE J. Sel. Areas Commun.* **2003**, *21*, 281–302. [CrossRef]
3. Votis, C.; Christofilakis, V.; Raptis, V.; Tatsis, G.; Chronopoulos, S.K.; Kostarakis, P. Design and analysis of a multiple-output transmitter based on DDS architecture for modern wireless communications. *AIP Conf. Proc.* **2010**, *1203*, 421–426.

4.　Kammoun, A.; Debbah, M.; Alouini, M.S. Design of 5G full dimension massive MIMO systems. *IEEE Trans. Commun.* **2018**, *66*, 726–740.

5.　Osseiran, A.; Boccardi, F.; Braun, V.; Kusume, K.; Marsch, P.; Maternia, M.; Queseth, O.; Schellmann, M.; Schotten, H.; Taoka, H.; et al. Scenarios for 5G mobile and wireless communications: The vision of the METIS project. *IEEE Commun. Mag.* **2014**, *52*, 26–35. [CrossRef]

6.　Angelis, C.T.; Chronopoulos, S.K. System performance of an LTE MIMO downlink in various fading environments. In Proceedings of the Ambient Media and Systems, Berlin, Germany, 27–28 January 2011; pp. 36–43.

7.　Ojaroudiparchin, N.; Shen, M.; Pedersen, G.F. Multi-layer 5G mobile phone antenna for multi-user MIMO communications. In Proceedings of the 23rd Telecommunications Forum (TELFOR), Belgrade, Serbia, 24–26 November 2015; pp. 559–562.

8.　Hassan, N.; Fernando, X. Massive MIMO Wireless Networks: An Overview. *Electronics* **2017**, *6*, 63. [CrossRef]

9.　Larsson, E.; Edfors, O.; Tufvesson, F.; Marzetta, T. Massive MIMO for next generation wireless Systems. *IEEE Commun. Mag.* **2014**, *52*, 186–195. [CrossRef]

10.　Yang, H.H.; Quek, T.Q.S. *Massive MIMO Meet Small Cell*; Springer Briefs in Electrical and Computer Engineering; Springer International Publishing: Basel, Switzerland, 2017.

11.　Sharawi, M.S. *Printed MIMO Antenna Engineering*; Artech House: Norwood, MA, USA, 2014.

12.　Parchin, N.O.; Basherlou, H.J.; Al-Yasir, Y.I.A.; Abd-Alhameed, R.A.; Abdulkhaleq, A.M.; Noras, J.M. Recent developments of reconfigurable antennas for current and future wireless communication systems. *Electronics* **2019**, *8*, 128. [CrossRef]

13.　Parchin, N.O.; Al-Yasir, Y.; Abdulkhaleq, A.M.; Elfergani, I.; Rayit, A.; Noras, J.M.; Rodriguez, J.; Abd-Alhameed, R.A. Frequency reconfigurable antenna array for mm-Wave 5G mobile handsets. In Proceedings of the 9th International Conference on Broadband Communications, Networks, and Systems, Faro, Portugal, 19–20 September 2018.

14.　Al-Yasir, Y.; Abdullah, A.; Ojaroudi Parchin, N.; Abd-Alhameed, R.; Noras, J. A new polarization-reconfigurable antenna for 5G applications. *Electronics* **2018**, *7*, 293. [CrossRef]

15.　Hussain, R.; Alreshaid, A.T.; Podilchak, S.K.; Sharawi, M.S. Compact 4G MIMO antenna integrated with a 5G array for current and future mobile handsets. *IET Microw. Antennas Propag.* **2017**, *11*, 271–279. [CrossRef]

16.　Chen, Q.; Lin, H.; Wang, J.; Ge, L.; Li, Y.; Pei, T. Single ring slot based antennas for metal-rimmed 4G/5G smartphones. *IEEE Trans. Antennas Propag.* **2019**, *67*, 1476–1487. [CrossRef]

17.　Ojaroudi Parchin, N.; Abd-Alhameed, R.A. A compact Vivaldi antenna array for 5G channel sounding applications. In Proceedings of the 12th European Conference on Antennas and Propagation, London, UK, 9–13 April 2018.

18.　Al-Hadi, A.A.; Ilvonen, J.; Valkonen, R.; Viikan, V. Eight-element antenna array for diversity and MIMO mobile terminal in LTE 3500MHz band. *Microw. Opt. Technol. Lett.* **2014**, *56*, 1323–1327. [CrossRef]

19.　Abdullah, M. Compact 4-Port MIMO antenna system for 5G mobile terminal. In Proceedings of the International Applied Computational Electromagnetics Society Symposium, Florence, Italy, 26–30 March 2017.

20.　Ojaroudi Parchin, N.; Al-Yasir, Y.I.A.; Abd-Alhameed, R.A.; Noras, J.M. Dual-polarized MIMO antenna array design using miniaturized self-complementary structures for 5G smartphone applications. In Proceedings of the EuCAP Conference, Krakow, Poland, 31 March–5 April 2019. accepted.

21.　Wong, K.L.; Lu, J.Y.; Chen, L.Y.; Li, W.Y.; Ban, Y.L. 8-antenna and 16-antenna arrays using the quad-antenna linear array as a building block for the 3.5-GHz LTE MIMO operation in the smartphone. *Microw. Opt. Technol. Lett.* **2016**, *58*, 174–181. [CrossRef]

22.　Rao, L.-Y.; Tsai, C.-J. 8-loop antenna array in the 5 inches size smartphone for 5G communication the 3.4 GHz–3.6 GHz band MIMO operation. In Proceedings of the Progress in Electromagnetics Research Symposium (PIERS), Toyama, Japan, 1–4 August 2018.

23.　Abdullah, M.; Ban, Y.L.; Kang, K.; Li, M.Y.; Amin, M. Eight-element antenna array at 3.5GHz for MIMO wireless application. *Prog. Electromagn. Res. C* **2017**, *78*, 209–217. [CrossRef]

24.　Li, Y.; Luo, Y.; Yang, G. High-isolation 3.5-GHz 8-antenna MIMO array using balanced open slot antenna element for 5G smartphones. *IEEE Trans. Antennas Propag.* **2019**. [CrossRef]

25.　Sun, L.; Feng, H.; Li, Y.; Zhang, Z. Compact 5G MIMO mobile phone antennas with tightly arranged orthogonal-mode pairs. *IEEE Trans. Antennas Propag.* **2018**, *66*, 6364–6369. [CrossRef]

26. Li, M.Y.; Ban, Y.L.; Xu, Z.Q.; Guo, J.; Yu, Z.F. Tri-polarized 12-antenna MIMO array for future 5G smartphone applications. *IEEE Access* **2018**, *6*, 6160–6170. [CrossRef]

27. Zhao, A.; Ren, Z. Size reduction of self-isolated MIMO antenna system for 5G mobile phone applications. *IEEE Antennas Wirel. Propag. Lett.* **2019**, *18*, 152–156. [CrossRef]

28. Statement: Improving Consumer Access to Mobile Services at 3.6 GHz to 3.8 GHz. Available online: https://www.ofcom.org.uk/consultations-and-statements/category-1/future-use-at-3.6-3.8-ghz (accessed on 21 October 2018).

29. *CST Microwave Studio*; ver. 2018; CST: Framingham, MA, USA, 2018.

30. Chang, K. *Microwave Ring Circuits and Antennas*; Wiley: New York, NY, USA, 1996.

31. Batchelor, J.C.; Langley, R.J. Microstrip annular ring slot antennas for mobile applications. *Electron. Lett.* **2019**, *32*, 1635–1636. [CrossRef]

32. Yoshimura, Y. A microstripline slot antenna. *IEEE Trans. Microw. Theory Tech.* **1972**, *20*, 760–762. [CrossRef]

33. Elfergani, I.; Hussaini, A.S.; Rodriguez, J.; Abd-Alhameed, R. *Antenna Fundamentals for Legacy Mobile Applications and Beyond*; Springer Nature: Basingstoke, UK, 2017; pp. 1–659.

34. Al-Nuaimi, M.K.T.; Whittow, W.G. Performance investigation of a dual element IFA array at 3 GHz for MIMO terminals. In Proceedings of the Antennas and Propagation Conference (LAPC), Loughborough, UK, 14–15 November 2011; pp. 1–5.

35. Nguyen, Q.D.; Le, T.T.; Le, D.T.; Tran, X.N.; Yamada, Y. A compact MIMO ultra-wide band antenna with low mutual coupling. *Appl. Comput. Electromagn. Soc. J.* **2018**, *31*, 252–260.

36. Parchin, N.O.; Al-Yasir, Y.I.; Ali, A.H.; Elfergani, I.; Noras, J.M.; Rodriguez, J.; Abd-Alhameed, R.A. Eight-element dual-polarized MIMO slot antenna system for 5G smartphone applications. *IEEE Access* **2019**, *9*, 15612–15622. [CrossRef]

37. Syrytsin, I.; Zhang, S.; Pedersen, G.F. Performance investigation of a mobile terminal phased array with user effects at 3.5 GHz for LTE advanced. *IEEE Antennas Wirel. Propag. Lett.* **2017**, *16*, 1847–1850. [CrossRef]

38. Sharawi, M.S. Printed multi-band MIMO antenna systems and their performance metrics [wireless corner]. *IEEE Antennas Propag. Mag.* **2013**, *55*, 218–232. [CrossRef]

39. Ojaroudi Parchin, N.; Alibakhshikenari, M.; Jahanbakhsh Basherlou, H.; AAbd-Alhameed, R.; Rodriguez, J.; Limiti, E. mm-Wave phased array quasi-Yagi antenna for the upcoming 5G cellular communications. *Appl. Sci.* **2019**, *9*, 978. [CrossRef]

40. Basar, M.R.; Malek, M.F.; Juni, K.M.; Saleh, M.I.; Idris, M.S.; Mohamed, L.; Saudin, N.; Mohd Affendi, N.A.; Ali, A. The use of a human body model to determine the variation of path losses in the human body channel in wireless capsule endoscopy. *Prog. Electromagn. Res.* **2013**, *133*, 495–513. [CrossRef]